LETTER

Signature of Fermi arc surface states in Andreev reflection at the WTe_2 Weyl semimetal surface

To cite this article: A. Kononov *et al* 2018 *EPL* **122** 27004

A Letters Journal Exploring the Frontiers of Physics

April 2018

EPL, **122** (2018) 27004 www.epljournal.org
doi: 10.1209/0295-5075/122/27004

Signature of Fermi arc surface states in Andreev reflection at the WTe_2 Weyl semimetal surface

A. Kononov[1], O. O. Shvetsov[1,2], S. V. Egorov[1], A. V. Timonina[1], N. N. Kolesnikov[1] and E. V. Deviatov[1]

[1] *Institute of Solid State Physics of the Russian Academy of Sciences - Chernogolovka, Moscow District, 2 Academician Ossipyan str., 142432 Russia*
[2] *Moscow Institute of Physics and Technology - Institutsky per. 9, Dolgoprudny, 141700 Russia*

received 10 April 2018; accepted in final form 28 May 2018
published online 19 June 2018

PACS 74.45.+c – Proximity effects; Andreev reflection; SN and SNS junctions
PACS 73.23.-b – Electronic transport in mesoscopic systems
PACS 73.40.-c – Electronic transport in interface structures

Abstract – We experimentally investigate charge transport through the interface between a niobium superconductor and a three-dimensional WTe_2 Weyl semimetal. In addition to classical Andreev reflection, we observe sharp non-periodic subgap resistance resonances. From an analysis of their positions, magnetic field and temperature dependences, we can interpret them as an analog of Tomasch oscillations for transport along the topological surface state across the region of proximity-induced superconductivity at the Nb-WTe_2 interface. The observation of distinct geometrical resonances implies a specific transmission direction for carriers, which is a hallmark of the Fermi arc surface states.

Introduction. – The recent interest in Weyl semimetals is mostly connected with topological surface properties [1]. Weyl semimetals are conductors which, like other topological materials [2–5], are characterized by topologically protected conducting surface states. The concept of Weyl semimetals has been extended to type-II materials [1], like $MoTe_2$ and WTe_2, where constant energy surfaces are open electron and hole pockets with a Weyl point at their touching. Weyl points are topologically protected and their projections on the surface Brillouin zone are connected by Fermi arc surface states. For these materials, surface states were demonstrated in several experiments [6–8], although their topological nature is still debatable [9,10]. In contrast to the three-dimensional topological insulators [2] described by Z_2 invariant, the Weyl surface states inherit the chiral property of the Chern insulator edge states [1].

Topological materials exhibit non-trivial physics in proximity to a superconductor [11–13]. For a single normal-superconductor (NS) contact, Andreev reflection [14] allows low-energy electron transport from normal metal to superconductor by creating a Cooper pair, so a hole is reflected back to the normal side of the junction [15, 16]. The process can be more complicated [17] if Andreev transport goes through an intermediate conductive region, *e.g.*, the topological surface state at the NS interface [18–20]. Also, geometrical resonances are predicted [21,22] within the topological surface state in proximity to a superconductor, analogously to the classical Tomasch [24–27] effect.

Here, we experimentally investigate charge transport through the interface between a niobium superconductor and a three-dimensional WTe_2 Weyl semimetal. In addition to classical Andreev reflection, we observe sharp non-periodic subgap resistance resonances. From an analysis of their positions, magnetic field and temperature dependences, we can interpret them as an analog of Tomasch oscillations for transport along the topological surface state across the region of proximity-induced superconductivity at the Nb-WTe_2 interface. The observation of distinct geometrical resonances implies a specific transmission direction for carriers, which is a hallmark of the Fermi arc surface states.

Samples and technique. – The WTe_2 compound was synthesized from elements by reaction of metal with tellurium vapor in the sealed silica ampule. The WTe_2 crystals were grown by the two-stage iodine transport [28], that previously was successfully applied [28,29] for growth of other metal chalcogenides like NbS_2 and $CrNb_3S_6$.

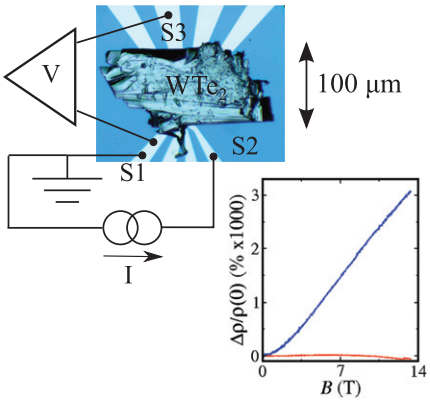

Fig. 1: (Color online) Sketch of the sample with niobium contacts to the bottom surface of a WTe_2 crystal. 70 nm thick niobium superconducting leads are formed on the insulating SiO_2 substrate. A WTe_2 single crystal is weakly pressed to the niobium leads pattern, forming planar Nb-WTe_2 junctions with $\approx 10 \times 10\,\mu m^2$ area. Charge transport is investigated in a standard three-point technique: the studied contact (S1) is grounded and two other contacts (S2 and S3) are used for applying current (below 100 μA) and measuring the WTe_2 potential. The inset demonstrates large positive magnetoresistance $\rho(B) - \rho(B = 0)/\rho(B = 0)$ for our WTe_2 samples at 1.2 K in the normal magnetic field (the blue curve), which goes to zero in the parallel one (the red curve), as has been shown for WTe_2 Weyl semimetal [30]. The current is parallel to the a-axis of WTe_2.

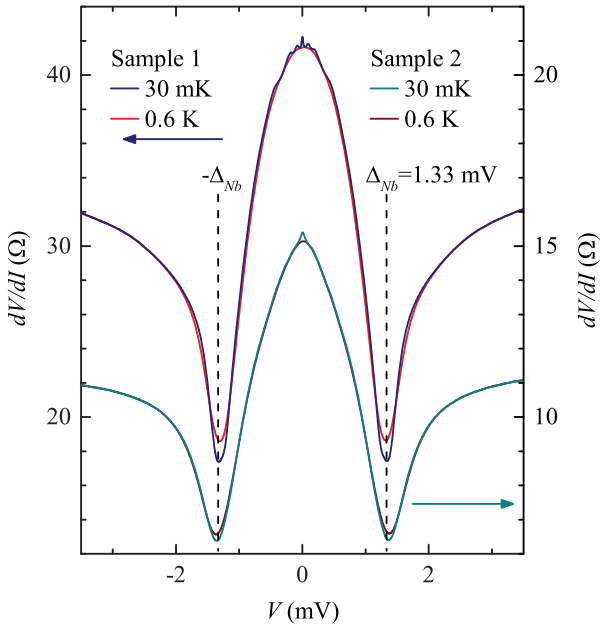

Fig. 2: (Color online) Examples of $dV/dI(V)$ characteristics for two Nb-WTe_2 junctions for two different temperatures. The niobium superconducting gap $\Delta_{Nb} \simeq \pm$ 1.33 mV is marked by dashed lines. The general behavior of $dV/dI(V)$ curves is not sensitive to temperature for $T \ll T_c = 9$ K.

The WTe_2 composition is verified by energy-dispersive X-ray spectroscopy. The X-ray diffraction (Oxford diffraction Gemini-A, MoKα) confirms the $Pmn2_1$ orthorhombic single crystal WTe_2 with lattice parameters $a = 3.48750(10)$ Å, $b = 6.2672(2)$ Å, and $c = 14.0629(6)$ Å.

A sample sketch is presented in fig. 1. We use dc magnetron sputtering to deposit a 70 nm thick niobium film on the insulating SiO_2 substrate. Superconducting leads are formed by the lift-off technique. A WTe_2 single crystal (≈ 0.5 mm $\times$ 100 μm $\times$ 0.5 μm dimensions) is weakly pressed to the niobium leads pattern, so the planar Nb-WTe_2 junctions (with $\approx 10 \times 10\,\mu m^2$ area) are formed at the bottom surface of the WTe_2 crystal.

We study electron transport across a single Nb-WTe_2 junction in a standard three-point technique, see fig. 1(c): the studied contact is grounded and two other contacts are used for applying current (below 100 μA) and measuring the WTe_2 potential. To obtain $dV/dI(V)$ characteristics, the dc current is additionally modulated by a low ac (0.5 μA, 1.2 kHz) component. We measure both, dc (V) and ac ($\sim dV/dI$) components of the WTe_2 potential by using a dc voltmeter and a lock-in, respectively. We check that the lock-in signal is independent of the modulation frequency in the 500–2500 Hz range, which is defined by applied ac filters.

To extract features specific to WTe_2 Weyl semimetal surface states, the measurements are performed in a dilution refrigerator covering 30 mK–1.2 K temperature range. We check by standard magnetoresistance measurements that our WTe_2 samples demonstrate large, non-saturating positive magnetoresistance $\rho(B) - \rho(B = 0)/\rho(B = 0)$ in the normal magnetic field, which goes to zero in the parallel one, see inset to fig. 1, as has been shown for the WTe_2 Weyl semimetal [30]. From the experimental curves, the sample is macroscopically homogeneous. We do not observe Shubnikov de Haas oscillations, so the mobility is smaller than in the best WTe_2 samples [30]. On the other hand, the bulk mobility value is not crucial for investigations of a single Nb-WTe_2 interface.

Experimental results. – Examples of $dV/dI(V)$ characteristics are shown in fig. 2 for two different junctions with different R_N. The obtained $dV/dI(V)$ curves are verified to be independent of the mutual positions of the current/voltage contacts, so they only reflect the transport parameters of the grounded Nb-WTe_2 junction.

The main $dV/dI(V)$ behavior is consistent with the standard one [15,16] of a single Andreev junction: every curve demonstrates a clearly defined superconducting gap $\Delta_{Nb} \simeq \pm$ 1.33 mV (denoted by dashed lines), which is in a good correspondence with the expected $T_c \approx 9$ K for niobium. Then the subgap resistance exceeds the normal resistance value, so single-particle scattering is significant at the Nb-WTe_2 interface, but it is undoubtedly finite, which is only possible due to Andreev reflection [16,19,20]. A transmission of the interface T can be estimated as $\approx$ 0.73–0.76 for these junctions, which corresponds to the BTK barrier strength [16] $Z \approx 0.6$. The interface

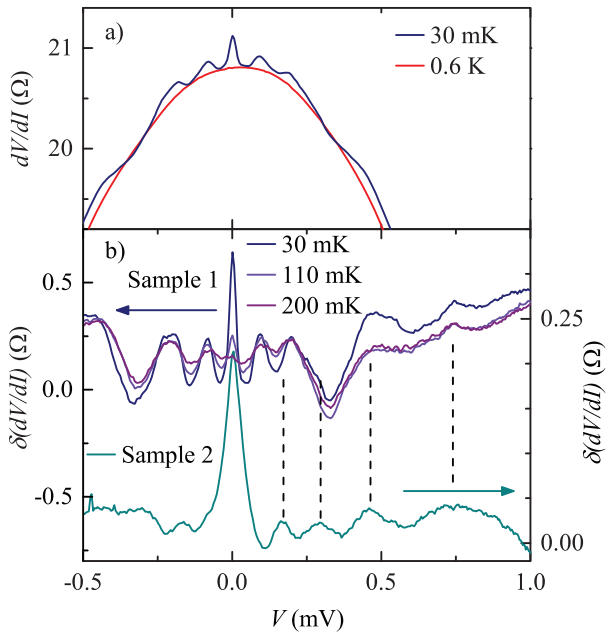

Fig. 3: (Color online) (a) The central part of $\mathrm{d}V/\mathrm{d}I(V)$ curves at 30 mK and 0.6 K temperatures. Specifics of Nb-WTe_2 junction appear in subgap resistance resonances below 0.6 K. (b) The difference $\delta(\mathrm{d}V/\mathrm{d}I(V))$ between $\mathrm{d}V/\mathrm{d}I(V)$ characteristics at low temperatures (30 mK, 110 mK, 200 mK) and after vanishing of resonances at 0.6 K. The positions of the resonances are denoted by dashed lines, they are non-periodic and concentrated strictly within the superconducting gap. $\mathrm{d}V/\mathrm{d}I$ is a maximum at zero bias for both Nb-WTe_2 junctions.

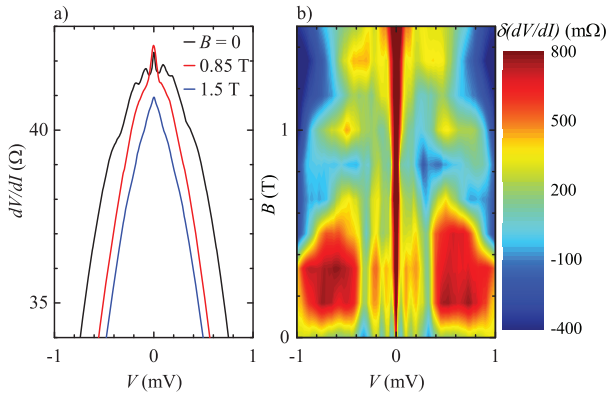

Fig. 4: (Color online) (a) Examples of $\mathrm{d}V/\mathrm{d}I(V)$ characteristics for different magnetic fields at low (30 mK) temperature. The resonances disappear completely above 0.85 T, while the zero-bias $\mathrm{d}V/\mathrm{d}I$ peak survives. At higher fields, the $\mathrm{d}V/\mathrm{d}I(V)$ curve still demonstrates a non-trivial shape, with non-zero first derivative at zero bias. (b) Colormap showing the evolution of $\delta(\mathrm{d}V/\mathrm{d}I(V))$ with magnetic field. The oscillations' positions are constant up to their disappearance above 0.85 T. Additional features appear in higher fields.

scattering is expected, since the sputtered niobium is natively oxidized prior to placing a WTe_2 single crystal onto the Nb leads pattern.

Specifics of the WTe_2 Weyl semimetal appear as sharp subgap resistance resonances, see figs. 2 and 3, which cannot be expected [15] for a single Andreev NS contact. The resonances are suppressed completely above 0.6 K. Since the general behavior of $\mathrm{d}V/\mathrm{d}I(V)$ curves is not sensitive to temperature much below $T_c = 9$ K, see fig. 2, the resonances can be analyzed in detail by subtracting the high-temperature (0.6 K) monotonous $\mathrm{d}V/\mathrm{d}I$ curve from the low-temperature (30 mK) one. The result ($\delta(\mathrm{d}V/\mathrm{d}I(V))$) is shown in fig. 3(b) for the junctions from fig. 2, the positions of the resonances are denoted by dashed lines. They are concentrated strictly within the superconducting gap and $\mathrm{d}V/\mathrm{d}I$ is a maximum at zero bias, the distance between the resonances is obviously increasing with bias in fig. 3(b). The number of visible resonances is different for different junctions. With increasing temperature, the amplitude of every resonance is diminishing, while its position is invariant, see fig. 3(b).

$\mathrm{d}V/\mathrm{d}I(V)$ curves are shown in fig. 4(a) for different magnetic fields, oriented along the a-axis of the WTe_2 crystal. In contrast to temperature suppression, the zero-bias $\mathrm{d}V/\mathrm{d}I$ peak survives above 0.85 T, while the resonances disappear completely. Moreover, the $\mathrm{d}V/\mathrm{d}I(V)$ curve still demonstrates a non-trivial shape even for higher fields, with the non-zero first derivative at zero bias, which also differs from temperature $\mathrm{d}V/\mathrm{d}I(V)$ suppression. This evolution is shown in fig. 4(b) as $\delta(\mathrm{d}V/\mathrm{d}I(V))$ colormap. The oscillations' positions are constant up to their disappearance at 0.85 T, while superconductivity is completely suppressed around 4 T magnetic field in our samples.

Discussion. – As a result, we observe pronounced subgap $|eV| < \Delta_{Nb}$ resonances for well-developed Andreev $\mathrm{d}V/\mathrm{d}I(V)$ curves for a single Nb-WTe_2 SN junction. In general, resonance conditions require particle propagation between two different (SN or NN) interfaces.

For a thin WTe_2 crystal, it is naturally to think about vertical transport, normal to the Nb-WTe_2 interface. In this case, both Tomasch [24,25] and MacMillan-Rowell [31,32] geometrical resonances could be anticipated, which originate [24,26,27,31,32] due to the space restriction in the S or N regions, respectively. However, these geometrical resonances should be observed at energies above the niobium superconducting gap, which contradicts the experimental observations in fig. 2. Also, MacMillan-Rowell oscillations [23,31,32] for bulk carriers in the WTe_2 crystal are strictly periodic, which is is obviously not the case in fig. 3.

Another possibility is multiple Andreev reflections (MAR) [15], but the experimental $\mathrm{d}V/\mathrm{d}I(V)$ curves are invariant to the choice of the potential contact. The resonance positions in fig. 3(b) does not correspond to the MAR sequence $E_n = 2\Delta_{Nb}/n, n = 1, 2, 3, \ldots$. Significant single-particle scattering at the Nb-WTe_2 interface is inconsistent with MAR observation conditions for highly separated (more then 5 μm) Nb contacts.

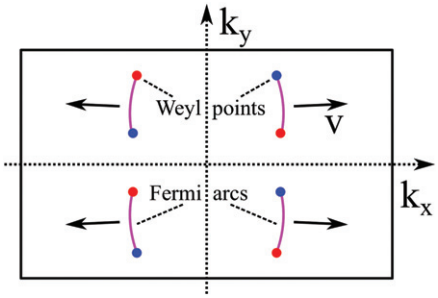

Fig. 5: (Color online) Sketch of Fermi arcs and projections of Weyl points on the (001) surface Brillouin zone. WTe_2 has eight Weyl points which are connected by four Fermi arcs, these arcs define two directions for carriers in the surface state. In WTe_2, the Weyl points are aligned along the *b*-axis [10] of the crystal, so these two directions merge into one along the *a*-axis, which defines a specific transmission direction of the carriers.

Thus, the observed resonances require a relation to surface states at the Nb-WTe_2 interface. WTe_2 is regarded as a type-II Weyl semimetal [7,30,33] hosting topological Fermi arcs states on (001) surfaces [34], which was demonstrated in several experiments [7,8]. In this case, an analog of Tomasch oscillations is allowed for transport along the topological surface state across the region of proximity-induced superconductivity near the niobium superconducting lead [21,22].

The resonances appear as Fabry-Perot–type transmission resonances for Bogoliubov quasiparticles in a long $l \gg \xi$ single NS junction, ξ is a coherence length. They are situated [21,22] at energies $eV_n = \sqrt{\Delta_{ind}^2 + (hv_f n/2l)^2}$, where $n = 0, 1, 2, \ldots$, v_F is the Fermi velocity. According to this relation, the induced gap Δ_{ind} is reflected by the zero-bias structure [17,18,20] in fig. 3. By fitting the resonance positions, we obtain $\Delta_{ind} \approx 0.1$ meV, the effective junction dimension as $l \approx 2\,\mu$m for $v_F \sim 1.5 \cdot 10^5 \frac{\mathrm{m}}{\mathrm{s}}$ (from ARPES data [9]).

This value is comparable with the dimensions of the planar Nb-WTe_2 junction (below $10\,\mu$m), taking in mind that placing WTe_2 on top of Nb does not guarantee good contact at all the surface. $l \sim 2\,\mu$m is also about the mean free path along the *a*-axis in WTe_2. It much exceeds the coherence length [35,36] $l \gg \xi = (l_e \times \hbar v_F^N / \pi \Delta_{in})^{1/2} \approx 200$ nm, which is obligatory to observe Tomasch oscillations for transport along the topological surface state [21,22].

The crucial point is that transmission resonances imply a well-defined junction length l. The obtained $\mathrm{d}V/\mathrm{d}I(V)$ curves are independent of the mutual positions of the current/voltage contacts, so they only reflect the transport near the Nb-WTe_2 interface. For the planar NS junction without axial symmetry (it is nearly rectangular in our case), l is different in different directions, which should smear the resonances for trivial surface states, *e.g.*, originating from band bending near the WTe_2 surface. On the other hand, Weyl surface states inherit the chiral property of the Chern insulator edge states [1], where the preferable directions are defined by Fermi arcs on a particular crystal surface. In WTe_2, the Weyl points are aligned along the *b*-axis [10] of the crystal, forming preferable directions for surface carriers along the *a*-axis, see fig. 5. Thus, the observation of sharp subgap resonances is specific for topological transport within the Fermi arc surface states at the Nb-WTe_2 interface. Since the resonances are defined by the interference effects, they are obviously suppressed in the magnetic field above 0.85 T, see fig. 4. However, the $\mathrm{d}V/\mathrm{d}I(V)$ curve evolution in higher fields is unusual for Andreev reflection and requires further investigations.

Conclusion. – As a conclusion, we experimentally investigate charge transport through the interface between a niobium superconductor and a three-dimensional WTe_2 Weyl semimetal. In addition to classical Andreev reflection, we observe sharp non-periodic subgap resistance resonances. From an analysis of their positions, magnetic field and temperature dependences, we can interpret them as an analog of Tomasch oscillations for transport along the topological surface state across the region of proximity-induced superconductivity at the Nb-WTe_2 interface. The observation of distinct geometrical resonances implies a specific transmission direction for carriers, which is a hallmark of the Fermi arc surface states.

* * *

We wish to thank V. T. Dolgopolov, V. A. Volkov, I. Gornyi, and A. S. Melnikov for fruitful discussions, and S. S. Khasanov for X-ray sample characterization. We gratefully acknowledge financial support by the RFBR project 16-02-00405 and RAS.

REFERENCES

[1] Armitage N. P., Mele E. J. and Ashvin Vishwanath, *Rev. Mod. Phys.*, **90** (2018) 15001
[2] Hasan M. Z. and Kane C. L., *Rev. Mod. Phys.*, **82** (2010) 3045.
[3] Qi X.-L. and Zhang S.-C., *Rev. Mod. Phys.*, **83** (2011) 1057.
[4] Bansil A., Lin H. and Das T., *Rev. Mod. Phys.*, **88** (2016) 021004.
[5] Chiu C.-K., Teo J. C., Schnyder A. P. and Ryu S., *Rev. Mod. Phys.*, **88** (2016) 035005.
[6] Deng K., Wan G., Deng P., Zhang K., Ding S., Wang E., Yan M., Huang H., Zhang H., Xu Z., Denlinger J., Fedorov A., Yang H., Duan W., Yao H., Wu Y., Fan S., Zhang H., Chen X. and Zhou S., *Nat. Phys.*, **12** (2016) 11051110.
[7] Wang Ch., Zhang Y., Huang J., Nie S., Liu G., Liang A., Zhang Yu., Shen B., Liu J., Hu C., Ding Y., Liu D., Hu Y., He S., Zhao L., Yu L., Hu J., Wei J., Mao Z., Shi Y., Jia X., Zhang F., Zhang S., Yang F., Wang Z., Peng Q., Weng H., Dai X., Fang Z., Xu Z., Chen C. and Zhou X. J., *Phys. Rev. B*, **94** (2016) 241119.

[8] Wu Y., Mou D., Jo N. H., Sun K., Huang L., Budko S. L., Canfield P. C. and Kaminski A., *Phys. Rev. B*, **94** (2016) 121113.

[9] Bruno F. Y., Tamai A., Wu Q. S., Cucchi I., Barreteau C., de la Torre A., McKeown Walker S., Riccò S., Wang Z., Kim T. K., Hoesch M., Shi M., Plumb N. C., Giannini E., Soluyanov A. A. and Baumberger F., *Phys. Rev. B*, **94** (2016) 121112.

[10] Li P., Wen Y., He X., Zhang Q., Xia C., Yu Z., Yang S., Zhu Z., Alshareef H. and Zhang X., *Nat. Commun.*, **8** (2017) 2150.

[11] Hart Sean, Ren Hechen, Wagner Timo, Leubner Philipp, Mhlbauer Mathias, Brne Christoph, Buhmann Hartmut, Molenkamp Laurens W. and Yacoby Amir, *Nat. Phys.*, **10** (2014) 638643.

[12] Pribiag Vlad S., Beukman Arjan J. A., Qu Fanming, Cassidy Maja C., Charpentier Christophe, Wegscheider Werner and Kouwenhoven Leo P., *Nat. Nanotechnol.*, **10** (2015) 593.

[13] Khanna Udit, Mukherjee Dibya Kanti, Kundu Arijit and Rao Sumathi, *Phys. Rev. B*, **93** (2016) 121409.

[14] Andreev A. F., *Sov. Phys. JETP*, **19** (1964) 1228.

[15] Tinkham M., *Introduction to Superconductivity*, 2d edition (McGraw-Hill, New York) 1996.

[16] Blonder G. E., Tinkham M. and Klapwijk T. M., *Phys. Rev. B*, **25** (1982) 4515.

[17] Heslinga D. R., Shafranjuk S. E., van Kempen H. and Klapwijk T. M., *Phys. Rev. B*, **49** ((1994) 10484.

[18] Wiedenmann J., Liebhaber E., Kübert J. S., Bocquillon E. Ames Ch., Buhmann H., Klapwijk T. M. and Molenkamp L. W., *Phys. Rev. B*, **96** (2017) 165302.

[19] Kononov A., Egorov S. V., Kvon Z. D., Mikhailov N. N., Dvoretsky S. A. and Deviatov E. V., *Phys. Rev. B*, **93** (2016) 041303.

[20] Kononov A., Kostarev V. A., Semyagin B. R., Preobrazhenskii V. V., Putyato M. A., Emelyanov E. A. and Deviatov E. V., *Phys. Rev. B*, **96** (2017) 245304.

[21] Adroguer P., Grenier C., Carpentier D., Cayssol J., Degiovanni P. and Orignac E., *Phys. Rev. B*, **82** (2010) 081303.

[22] Kopnin N. B. and Melnikov A. S., *Phys. Rev. B*, **84** (2011) 064524.

[23] Shvetsov O. O., Kostarev V. A., Kononov A., Golyashov V. A., Kokh K. A., Tereshchenko O. E. and Deviatov E. V., *EPL*, **119** (2017) 57009.

[24] Tomasch W. J., *Phys. Rev. Lett.*, **16** (1966) 16.

[25] McMillan W. L. and Anderson P. W., *Phys. Rev. Lett.*, **16** (1966) 85.

[26] Nesher O. and Koren G., *Phys. Rev. B*, **60** (1999) 9287.

[27] Visani C., Sefrioui Z., Tornos J., Leon C., Briatico J., Bibes M., Barthélémy A., Santamara J. and Villegas Javier E., *Nat. Phys.*, **8** (2012) 539.

[28] Borisenko E. B., Berezin V. A., Kolesnikov N. N., Gartman V. K., Matveev D. V. and Shakhlevich O. F., *Phys. Solid State*, **59** (2017) 1310.

[29] Sidorov A., Petrova A. E., Pinyagin A. N., Kolesnikov N. N., Khasanov S. S. and Stishov S. M., *J. Exp. Theor. Phys.*, **122** (2016) 1047.

[30] Ali Mazhar N., Xiong Jun, Flynn Steven, Tao Jing, Gibson Quinn D., Schoop Leslie M., Liang Tian, Haldolaarachchige Neel, Hirschberger Max, Ong N. P. and Cava R. J., *Nature*, **514** (2014) 205.

[31] Rowell J. M. and McMillan W. L., *Phys. Rev. Lett.*, **16** (1966) 453.

[32] Rowell J. M., *Phys. Rev. Lett.*, **30** (1973) 167170.

[33] Wang Y. *et al.*, *Nat. Commun.*, **7** (2016) 13142.

[34] Soluyanov A. A., Gresch D., Wang Z., Wu Q., Troyer M., Dai X. and Bernevig B. A., *Nature*, **527** (2015) 495.

[35] Kulik I. O., *Sov. Phys. JETP*, **30** (1970) 944.

[36] Dubos P., Courtois H., Pannetier B., Wilhelm F. K., Zaikin A. D. and Schön G., *Phys. Rev. B*, **63** (2001) 064502.